☙

Graphene and few-layer graphite probed by second-harmonic generation: Theory and experiment

Jesse J. Dean[*] and Henry M. van Driel

Department of Physics and Institute for Optical Sciences, University of Toronto, Toronto, Ontario, Canada M5S-1A7
(Received 16 June 2010; revised manuscript received 15 July 2010; published 8 September 2010)

We have measured second-harmonic generation (SHG) from graphene and other graphitic films, from two layers to bulk graphite, at room temperature; all samples are mounted on a 300 nm oxide layer of a Si(001) substrate. With 800 nm, 150 fs fundamental pulses, the anisotropic response was recorded for combinations of *p*-, *s*-, and diagonally polarized fundamental and second-harmonic beams as the samples were rotated about their normal. Graphene samples display SHG signatures only slightly different from that of the bare substrate which shows SHG with fourfold rotational symmetry. All other layered systems show threefold symmetry, although the ratio of isotropic to anisotropic response varies with the number of layers. A model based on linear light propagation in layered media with interface dipole and bulk quadrupole SHG sources is presented for the analysis. We show that data from all layered samples can be understood in terms of well-known linear optical properties, the SHG response of the bare substrate and four independent, complex nonlinear dipole susceptibility tensor elements of the graphene/air interface.

I. INTRODUCTION

In the last few years, there has been intense research into graphene and few-layer graphitic films (hereafter referred to collectively as C-films), both to study fundamental physics and to develop new nanoelectronic devices. Since one can easily obtain C-films with any integer number of layers, they offer a unique opportunity to determine how nonlinear optical properties of a layered system evolve, in this case from atomically thin graphene to bulk graphite. In this paper, we report experimental results for second-harmonic generation (SHG) from this family of layered materials, all mounted on an oxidized Si(001) substrate. With a 800 nm, 150 fs fundamental beam, the SHG is measured as a function of azimuthal rotation angle of the sample. A model based on linear light propagation in a layered system with interface dipole and bulk quadrupole sources is developed and used to analyze the SHG behavior.

Graphene is an atomically thin layer of hexagonally arranged carbon atoms. When stacked in a Bernal (*AB*) arrangement, it forms natural graphite. Here, we use micromechanical exfoliation to make graphene and other C-films. This involves mechanically cleaving flakes of natural graphite (e.g., using tape), and depositing them on a substrate, silicon with a layer of SiO_2, which makes the graphene visible.[1,2] This technique typically generates C-films tens of microns across. Exfoliated graphene and multilayered films are nearly defect free, and are only weakly bonded to the substrate.[3] However, exfoliated samples are generally only useful for fundamental science research due to the small sizes of the samples produced, as well as the inability to control the film thickness. Multilayer graphene of large area can be made using an epitaxial growth technique, involving the vacuum graphitization of SiC at high temperatures.[4,5] This typically generates 5–40 layers of graphene, although there is usually a non-negligible degree of disorder/defects in the lattice; the stacking arrangement is not hexagonal-Bernal, and the layer next to the SiC is often doped (metallic).

Several optical techniques are commonly used to obtain the properties of C-films. Graphene absorbs ~2% of near-infrared and visible light, making it difficult to detect optically. When placed on a layered substrate (e.g., 300 nm SiO_2 on Si as is used here), interference effects make few-layer C-films optically visible, and the number of layers may be determined exactly for sufficiently thin samples.[1,2] Raman spectroscopy is also commonly used to discriminate between one, two, and three layers, and also to characterize defects.[6,7] Optical pump-probe techniques have been used to analyze the carrier cooling dynamics of photoexcited carriers in both epitaxial and exfoliated graphene.[8,9]

Nonlinear optical processes are known to provide insight into material properties, such as structural symmetry or band structure.[10–14] A notable example is the use of SHG to probe surfaces of centrosymmetric media. Because dipolar SHG is symmetry forbidden in the bulk of such media, the two dominant contributions are a surface-dipole-induced SHG, and a bulk-quadrupole contribution. The surface dipole contribution is often stronger, thus making SHG a useful surface probe of structural, charge transfer, and adsorbate effects. There has been little experimental investigation into the nonlinear optical properties of graphene and other C-films. However, as we have shown earlier, SHG from graphene mounted on an oxidized silicon substrate shows strikingly different symmetry characteristics than that from bilayer or bulk graphite.[15] In this paper, we offer a comprehensive set of results from SHG experiments on the family of C-films mounted on an oxidized Si substrate and a theoretical analysis of those results. The SHG intensity depends on the number of layers, the polarizations involved, and azimuthal angle of sample rotation. Using known linear optical properties and film thickness, we show that all results can be understood in terms of four complex dipolar nonlinear susceptibility tensor elements that govern the graphene/air interface.

The remainder of this paper is organized as follows: the following section gives the theoretical basis for describing SHG from a C-film/SiO_2/Si multilayer system, Sec. III describes the experimental setup used to observe SHG from the family of layered systems while Sec. IV gives the experi-

mental results and the extracted graphene/air surface dipolar tensor elements. This is followed by some conclusions.

II. SURFACE SHG THEORY

The samples we consider theoretically and experimentally consist of C-films of various layer thickness mounted on a 300 nm SiO_2 layer on a Si(001) substrate in air at room temperature. Although there may be some degree of surface roughness to the C-film and substrate, the substrate is known to be smooth at the scale of the wavelengths involved, and it is assumed that the C-film conforms to the substrate surface. We therefore treat all samples as being optically flat. A laser beam with frequency ω, which is incident on a sample at an angle θ, generates second-harmonic polarization sheets through dipolar effects at all interfaces (above the C-film, between the C-film and the SiO_2, and between the SiO_2 and the Si). There is possibly a bulk quadrupolar contribution from the C-film and a similar contribution from the Si. However, in the latter case since we do not intend to examine the SHG from the substrate in detail, all SHG from the substrate will be treated phenomenologically as originating from the top of the Si, generated by the downward propagating field immediately above the Si.

Depending on the crystal symmetry involved, it can be difficult to separate the surface and bulk contributions. Graphite is in the D_{6h}^4 space group; it has a threefold axis of symmetry, as well as a sixfold screw axis (a vertical shift of one layer spacing, followed by a 60° rotation leaves it unchanged). Therefore, the surface has threefold rotational symmetry (C_{3v}) while the bulk effectively has sixfold rotational symmetry. A rank-3 tensor (nonlinear susceptibility associated with dipole-induced SHG) can be sensitive to a threefold rotational symmetry whereas a rank-4 tensor (nonlinear susceptibility associated with quadrupole-induced SHG) is not sensitive to a sixfold rotational symmetry. Therefore, any bulk-quadrupole contribution to the SHG from the bulk of a C-film is isotropic with respect to an axial rotation. Furthermore, it is known that under either p- or s-polarized illumination, there is no isotropic s-polarized bulk quadrupole SHG.[11] Finally, any bulk contribution scales with the sample thickness, and therefore approaches zero in the thin-film limit. In our analysis, the bulk contribution is assumed to be significantly smaller than the surface and interface contributions, and is ignored. A failure in this approximation would manifest itself as a discrepancy between the theory and experimental results for thicker samples. We come back to this assumption below.

To describe all the interface SHG contributions, we use the transfer matrix method and Green's function formalism suggested by Sipe *et al.*[11,16] The SHG from an interface between two media may be treated as originating from either media (that is, the dipolar polarization sheet may be treated as being above or below the interface). In calculating the SHG, the fundamental E-field may be evaluated above or below the interface. Any combination of these describes the same physical process, but must use a different (renormalized) nonlinear susceptibility tensor to be consistent. One convenient standard is the vacuum interface model suggested
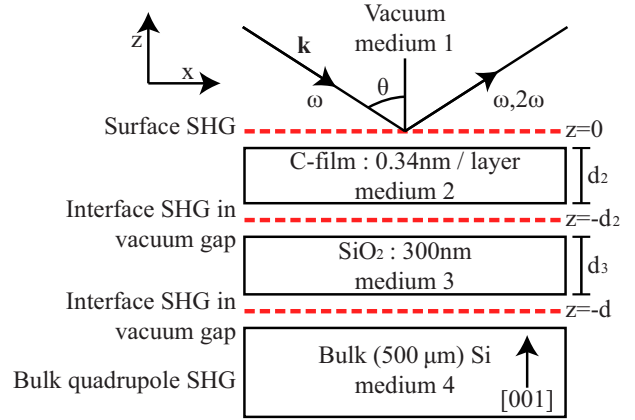

FIG. 1. (Color online) Diagram of interface structure including hypothetical vacuum interface in which the surface SHG occurs. A possible bulk contribution from the C-film is ignored.

by Gielis *et al.*[17] whereby the fundamental fields are calculated and produce an SHG polarization sheet in an infinitesimal vacuum gap between the media. Note that the presence of an infinitesimal vacuum gap will not change any linear propagation effects. From surface to substrate, the system is modeled as follows (Fig. 1): a 2ω polarization sheet above the top surface at $z=0$ (medium 1, effectively vacuum), a C-film of thickness $d_2=0.34$ nm $\times$ number of layers (medium 2), an infinitesimally thin vacuum interface containing a second 2ω polarization sheet at $z=-d_2$, a layer of SiO_2 of thickness $d_3=300$ nm (medium 3), a second vacuum interface containing a 2ω polarization sheet at $z=-d$, and finally bulk Si(001) (medium 4). Both the surface and bulk Si contributions are treated phenomenologically as being generated in the Si.

The z direction is defined to be the surface normal, and the beam propagates in the x-z plane with propagation constant $\mathbf{k}$. The determination of the SHG field involves four steps: calculation of the fundamental E-fields at the three relevant interfaces (above the top surface, between the C-film and the SiO_2, and the downward propagating component in the SiO_2/Si interface), determining the SHG polarization induced in the top two interfaces and the top of the Si in terms of the incident E-field and the interface nonlinear susceptibility tensor elements, calculating the radiated E-field from each SHG source, and finally adding them coherently.

To determine the effects of propagation, it is necessary to consider the index of refraction. Because the index of refraction is usually defined for a bulk medium, it is not clear if an index of refraction has physical meaning for a medium only a few atoms thick (graphene or few-layer graphite). However, when analyzing the reflection from thin C-films on oxidized Si, Blake *et al.* noted that graphene may be treated optically as bulk graphite with a thickness of 0.34 nm (the extension of the π orbitals out of plane) and that multilayer C-films may be treated similarly.[1] While the ordinary index of refraction (o) is easily measured, the extraordinary index of refraction (e) of graphite is difficult to measure, and there are variations reported in the literature. The values used here are obtained from the Handbook of Optical Constants of Sol-

ids, and references therein using the assumption that there are no significant features near the wavelengths used here.[18] For an incident fundamental wavelength of 800 nm, these are: $n_{2,o}(\omega)=3.08+1.88i$, $n_{2,e}(\omega)=1.37$, $n_{2,o}(2\omega)=2.62+1.29i$, and $n_{2,e}(2\omega)=1.35$. The accepted indices of refraction of the other media (air, SiO$_2$, Si) are readily available: $n_1(\omega)=n_1(2\omega)=1$, $n_3(\omega)=1.45$, $n_3(2\omega)=1.47$, $n_4(\omega)=3.71+0.0085i$, and $n_4(2\omega)=5.67+0.37i$ where the subscript refers to the medium.

A. Fundamental beam propagation

First, it is necessary to determine the fundamental E-fields above the top surface and in each vacuum interface. The E-field in any medium u, in full form, is the sum of those generated by the upward (+) and downward (−) propagating fields of s and p polarization,

$$\mathbf{E}_{u\pm}(\mathbf{r}) = (\hat{\mathbf{s}}E^s_{u\pm} + \hat{\mathbf{p}}_{u\pm}E^p_{u\pm})e^{ik_{uz}z}e^{ik_xx}. \tag{1}$$

The spatial phase dependence of the E-field ($\mathbf{k}_u \cdot \mathbf{r}$), which is defined as propagating in the x-z plane, has been split into its z component ($k_{uz}z$) and x component (k_xx); if all interfaces are parallel to the x-y plane, k_x does not depend on the medium. The direction of the p-polarized field $\hat{\mathbf{p}}_{\pm}E^p_{\pm}$ explicitly depends on whether it is upward (+) or downward (−) propagating whereas the direction of the s-polarized field $\hat{\mathbf{s}}E^s_{\pm}$ does not. Using the axes defined above, these directions are

$$\hat{\mathbf{p}}_{\pm} = \frac{k_x\hat{\mathbf{z}} \mp k_{uz}\hat{\mathbf{x}}}{|\mathbf{k}_u|},$$

$$\hat{\mathbf{s}} = \hat{\mathbf{y}}. \tag{2}$$

The E-field may therefore be described using the vector

$$\mathbf{e}_u(z) = \begin{bmatrix} e_{u+}(z) \\ e_{u-}(z) \end{bmatrix} = \begin{bmatrix} E_{u+}e^{ik_{uz}z} \\ E_{u-}e^{-ik_{uz}z} \end{bmatrix}. \tag{3}$$

The top(bottom) element is the upward (downward) propagating field in medium u. The s and p polarizations are treated separately. The E-fields at various depths may then be related using the product of transfer matrices, $\bar{\mathbf{m}}_{uv}$ at an interface between medium u and v, and $\bar{\mathbf{m}}_u(d_u)$ for propagation through medium u of thickness d_u. The transfer matrices are given by

$$\bar{\mathbf{m}}_u(d_u) = \begin{bmatrix} e^{ik_{uz}d_u} & 0 \\ 0 & e^{-ik_{uz}d_u} \end{bmatrix},$$

$$\bar{\mathbf{m}}_{uv} = \frac{1}{t_{uv}} \begin{bmatrix} 1 & r_{uv} \\ r_{uv} & 1 \end{bmatrix}. \tag{4}$$

Here, r_{uv} and t_{uv} are the Fresnel reflection and transmission coefficients for the u to v interface. Note that t_{uv}, r_{uv}, and k_{uz} depend on the polarization, and in the case of p-polarization, both the ordinary and extraordinary indices of refraction. The transfer matrix through a composite system is the product of the transfer matrices of each element. At opposite ends of a composite system (i.e., from medium 1 at $z=0$ to medium 4 at $z=-d$), the E-fields are related by $\mathbf{e}_1(0)=\bar{\mathbf{m}}_{14}\mathbf{e}_4(-d)$, where

$\bar{\mathbf{m}}_{14}=\bar{\mathbf{m}}_{12}\bar{\mathbf{m}}_2(d_2)\bar{\mathbf{m}}_{23}\bar{\mathbf{m}}_3(d_3)\bar{\mathbf{m}}_{34}$. Therefore, the composite transfer matrix for the system may be written in terms of the total effective transmission and reflection coefficients,

$$\bar{\mathbf{m}}_{14} = \frac{1}{t^{eff}_{14}} \begin{bmatrix} t^{eff}_{14}t^{eff}_{41} - r^{eff}_{14}r^{eff}_{41} & r^{eff}_{14} \\ -r^{eff}_{41} & 1 \end{bmatrix}. \tag{5}$$

At position z, the total field in each direction is

$$E_y = e^s_+(z) + e^s_-(z),$$

$$E_z = [e^p_+(z) + e^p_-(z)]\sin(\theta),$$

$$E_x = [-e^p_+(z) + e^p_-(z)]\cos(\theta). \tag{6}$$

Above the top surface, the E-field is the incident field E_{1-} propagating downwards and its reflection,

$$\mathbf{e}_1(0) = \begin{bmatrix} r^{eff}_{14} \\ 1 \end{bmatrix} E_{1-}, \tag{7}$$

where the reflection coefficient may be found from Eq. (5) to be $r^{eff}_{14}=\frac{m^{1,2}_{14}}{m^{2,2}_{14}}$, and the superscripts for m refer to the row and column number. The E-field components can then be directly calculated using Eq. (6).

The E-field in the first and second vacuum interfaces can be calculated in a similar manner,

$$\mathbf{e}_1(-d_2) = \bar{\mathbf{m}}_{12}\bar{\mathbf{m}}_2(-d_2)\bar{\mathbf{m}}_{21}\mathbf{e}_1(0) \tag{8}$$

for the first vacuum interface, and

$$\mathbf{e}_1(-d) = \bar{\mathbf{m}}_{13}\bar{\mathbf{m}}_3(-d_3)\bar{\mathbf{m}}_{32}\bar{\mathbf{m}}_2(-d_2)\bar{\mathbf{m}}_{21}\mathbf{e}_1(0) \tag{9}$$

for the second vacuum interface, and the E-field above the top surface, $\mathbf{e}_1(0)$, has been determined from Eq. (7).

B. Nonlinear susceptibility tensor elements

At the top surface of the C-film, the dipolar source for SHG is $\mathbf{P}=\bar{\mathbf{\Delta}}'(\phi)\mathbf{E}_1\mathbf{E}_1\delta(z_+)$, where $\mathbf{E}_1$ is the fundamental E-field above the surface, and the delta function implies an SHG polarization plane immediately above the top surface. The tensor $\bar{\mathbf{\Delta}}'(\phi)$ is the second-harmonic dipolar susceptibility tensor $\bar{\mathbf{\Delta}}$ specific to the C_{3v} symmetry of the surface of a multilayered C-film, rotated about an angle ϕ relative to the standard crystal axis (mirror plane perpendicular to $\hat{\mathbf{y}}$). This tensor has four independent nonzero elements: ∂_{11}, ∂_{15}, ∂_{31}, and ∂_{33}. The polarization density (neglecting the spatial dependence for now) may be written in the standard notation as

$$\mathbf{P} = \begin{bmatrix} P_x \\ P_y \\ P_z \end{bmatrix} = \begin{bmatrix} \cos(3\phi)\partial_{11}^t & -\cos(3\phi)\partial_{11}^t & 0 & 0 & \partial_{15}^t & -\sin(3\phi)\partial_{11}^t \\ -\sin(3\phi)\partial_{11}^t & \sin(3\phi)\partial_{11}^t & 0 & \partial_{15}^t & 0 & -\cos(3\phi)\partial_{11}^t \\ \partial_{31}^t & \partial_{31}^t & \partial_{33}^t & 0 & 0 & 0 \end{bmatrix} \begin{bmatrix} E_x^2 \\ E_y^2 \\ E_z^2 \\ 2E_yE_z \\ 2E_xE_z \\ 2E_xE_y \end{bmatrix}. \tag{10}$$

The t superscript refers to the fact that this is specific to the top surface (air/C-film interface). Graphene, in contrast, has C_{6v} symmetry. In that case, the tensor is the same with the exception that $\partial_{11}^t = 0$ and it is immediately clear that the anisotropy vanishes.

From the bottom surface of the C-film (C-film/SiO$_2$ interface), the same symmetries apply since the SiO$_2$ is amorphous. The same equations may be used with t replaced with b, indicating possibly different susceptibility elements. It is known, however, that the film is only weakly (van der Waals) bonded to the SiO$_2$ so a reasonable simplification is to assume that the tensor is the same as that for the top surface. Because the z axis is flipped (C-film above, rather than below the polarization sheet), the substitutions become

$$\partial_{11} = \partial_{11}^t = \partial_{11}^b,$$

$$\partial_{31} = \partial_{31}^t = -\partial_{31}^b,$$

$$\partial_{33} = \partial_{33}^t = -\partial_{33}^b,$$

$$\partial_{15} = \partial_{15}^t = -\partial_{15}^b. \tag{11}$$

Of particular note is the infinitesimally thin case which applies (approximately) to monolayer and bilayer graphene: the SHG is associated with a single tensor which is the sum of the top and bottom tensors. For few-atom-thick samples, it is unclear if the SHG should be treated as originating from two separate polarization sheets instead of one, or whether these polarization sheets are determined by the same set of nonlinear tensor elements as for thicker samples. A single polarization sheet (and nonlinear susceptibility tensor) can always be used to model the measured SHG but then the tensor elements depend on the number of layers. However, a polarization sheet would be expected to be located in the center of the C-film, and in this case, one may not expect any SHG due to inversion symmetry for graphene and bilayer graphene. Without examining the microscopic origin of the SHG, we will show that a theory with equal tensor elements for both surfaces is sufficient for any number of layers. A failure in this assumption (i.e., if the tensor elements are different for few-layer samples) will manifest as a divergence between theory and experiment for thin samples (likely $< \sim 10$ layers, at which point the properties of graphene have evolved to those of bulk graphite).

For graphene, the infinitesimally thin limit gives exactly zero for all tensor elements. Physically, the SHG generated from the top surface is exactly out of phase with that generated from the bottom surface. Note that if one considers a single polarization sheet, an isotropic SHG signal would result. An inversion symmetry argument would give zero SHG from graphene. For a multilayer C-film, this gives a purely anisotropic tensor—all terms independent of ϕ are zero, while all terms which depend on ϕ are doubled, thus generating an E-field of the form $E \propto \cos(3\phi)$ or $\sin(3\phi)$ depending on which polarizations are involved. An inversion symmetry argument would necessarily apply to both graphene and bilayer graphene, therefore any SHG from bilayer graphene disproves an inversion symmetry argument for thin films. The infinitesimally thin limit implies a zero-absorption and zero-depth film, and is not reached even in the case of graphene, which absorbs $\sim 2\%$. However, this implies that graphene may only generate a very weak isotropic SHG signal, in agreement with previous results.[15] Furthermore, it is expected that few-layer C-films only generate a strong three-fold symmetric SHG signal with a weak isotropic component which is also in agreement with previous results. The agreement between the qualitative theoretical and experimental results suggests that this model (interference between two polarization sheets) is sufficient to describe SHG rather than a model with one polarization sheet with thickness-dependent tensor elements.

The SHG from the substrate is treated phenomenologically, and thus it is not necessary to consider the form of the tensor. We assume only that the radiated SHG is fourfold symmetric.

C. Radiated SHG

The fundamental E-fields at the relevant depths have been calculated in terms of the incident field, and the SHG polarizations have been calculated in terms of the fundamental E-fields. Next, it is necessary to calculate the E-fields generated by the 2ω polarization sheets and, using the transfer matrix formalism, determine the SHG radiated through the top of the sample.

Since fields at frequency ω and 2ω are considered in the following sections, lower-case quantities ($\bar{\mathbf{m}}$ and $\mathbf{k}$) refer to ω fields, and upper-case variables (including the polarization $\mathbf{P}$) refer to 2ω fields. E-fields (E and $\mathbf{e}$) follow the same notation as defined in Eqs. (1) and (3) since the implied frequency is clear. Polarization directions ($\hat{\mathbf{s}}$ and $\hat{\mathbf{p}}_{\pm}$) are independent of frequency.

A polarization sheet in a vacuum generates an upward (+) and downward (−) propagating wave with fields[16]

$$\mathbf{E}_{\pm} = E_{s\pm}\hat{\mathbf{s}} + E_{p\pm}\hat{\mathbf{p}}_{\pm},$$

$$E_{s\pm} = \frac{iK^2}{2K_z\varepsilon_0}\hat{\mathbf{s}}\cdot\mathbf{P},$$

$$E_{p\pm} = \frac{iK^2}{2K_z\varepsilon_0}\hat{\mathbf{p}}_{\pm}\cdot\mathbf{P}, \tag{12}$$

where $K = 2\omega/c$ is the wave number in air and $K_z = K\cos(\theta)$.

The SHG radiated from the top surface is the sum of the upward propagating wave and the reflected part of the downward propagating wave. This may be calculated using the transfer matrix formalism, with a discontinuity in the E-field corresponding to the polarization sheet. If the polarization sheet is defined to be sandwiched between $z=0^+$ and $z=0^-$, which is immediately above the top surface, then

$$\mathbf{e}_1(0^-) = \bar{\mathbf{M}}_{14}\mathbf{e}_4(-d),$$

$$\mathbf{e}_1(0^+) = \mathbf{v} + \mathbf{e}_1(0^-), \tag{13}$$

where $\mathbf{e}_4(-d)$ is the E-field at the top of the Si, $\mathbf{e}_1(0^+)$ is the E-field above the system, $\bar{\mathbf{M}}_{14}$ is the composite matrix from Eq. (5), and $\mathbf{v}$ is the discontinuity produced from the polarization sheet from Eq. (12),

$$\mathbf{v}_s = \frac{iK^2}{2K_z\varepsilon_0}\begin{bmatrix} \hat{\mathbf{s}}\cdot\mathbf{P} \\ -\hat{\mathbf{s}}\cdot\mathbf{P} \end{bmatrix},$$

$$\mathbf{v}_p = \frac{iK^2}{2K_z\varepsilon_0}\begin{bmatrix} \hat{\mathbf{p}}_+\cdot\mathbf{P} \\ -\hat{\mathbf{p}}_-\cdot\mathbf{P} \end{bmatrix}. \tag{14}$$

Through algebraic substitution, with the fact that $\mathbf{e}_1(0^+)$ has no downward propagating component, it is possible to solve for its upward propagating component $E_t^{2\omega}$ to obtain

$$E_{s,t}^{2\omega} = \frac{iK^2}{2K_z\varepsilon_0}P_y\left(1 + \frac{M_{14s}^{1,2}}{M_{14s}^{2,2}}\right),$$

$$E_{p,t}^{2\omega} = \frac{iK^2}{2K_z\varepsilon_0}\left[\left(\frac{M_{14p}^{1,2}}{M_{14p}^{2,2}} + 1\right)K_xP_z + \left(\frac{M_{14p}^{1,2}}{M_{14p}^{2,2}} - 1\right)K_zP_x\right]. \tag{15}$$

The 2ω polarizations can then be used to find the radiated E-field generated from the top surface. For simplicity, we consider only incident and emitted s or p polarization. The s- and p-polarized E-fields generated from a g-polarized (g is s or p) fundamental field are a sum of products of nonlinear tensor elements $\mathring{d}_x^f$ where $x = (11)$, (15), (31), and (33), and linear terms a, b, and c

$$\frac{E_{gs,t}^{2\omega}}{(E_g^{\omega})^2} = Fc_{t,11}^{gs}\mathring{d}_{11}^f\sin(3\phi),$$

TABLE I. Radiated E-field coefficients from top surface.

$$c_{t,11}^{ss} = \left(1 + \frac{M_{14s}^{1,2}}{M_{14s}^{2,2}}\right)(r_{14s}^{eff} + 1)^2$$

$$c_{t,11}^{ps} = -\left(1 + \frac{M_{14s}^{1,2}}{M_{14s}^{2,2}}\right)(-r_{14p}^{eff} + 1)^2\cos^2(\theta)$$

$$b_{t,11}^{sp} = -\left(\frac{M_{14p}^{1,2}}{M_{14p}^{2,2}} - 1\right)\cos(\theta)(r_{14s}^{eff} + 1)^2$$

$$b_{t,11}^{pp} = \left(\frac{M_{14p}^{1,2}}{M_{14p}^{2,2}} - 1\right)(-r_{14p}^{eff} + 1)^2\cos^3(\theta)$$

$$a_{t,31}^{sp} = \left(\frac{M_{14p}^{1,2}}{M_{14p}^{2,2}} + 1\right)(-r_{14p}^{eff} + 1)^2\sin(\theta)\cos^2(\theta)$$

$$a_{t,31}^{pp} = \left(\frac{M_{14p}^{1,2}}{M_{14p}^{2,2}} + 1\right)(-r_{14p}^{eff} + 1)^2\sin(\theta)\cos^2(\theta)$$

$$a_{t,33}^{pp} = \left(\frac{M_{14p}^{1,2}}{M_{14p}^{2,2}} + 1\right)(r_{14p}^{eff} + 1)^2\sin^3(\theta)$$

$$a_{t,15}^{pp} = 2\left(\frac{M_{14p}^{1,2}}{M_{14p}^{d}} - 1\right)(-r_{14p}^{eff} + 1)\cos^2(\theta)\sin(\theta)(r_{14p}^{eff} + 1)$$

$$\frac{E_{gp,t}^{2\omega}}{(E_g^{\omega})^2} = F\left[b_{t,11}^{gp}\mathring{d}_{11}^f\cos(3\phi) + \sum_x a_{t,x}^{gp}\mathring{d}_x^f\right],$$

where

$$F = \frac{iK^2}{2K_z\varepsilon_0}. \tag{16}$$

The coefficients are listed in Table I.

The SHG contribution from the vacuum interface may be calculated similarly. If the SHG polarization is on the plane $z = -d_2$ which is inside the infinitesimally thin vacuum interface, then the E-fields across the structure are

$$\mathbf{e}_1(0) = \bar{\mathbf{M}}_{12}\bar{\mathbf{M}}_2(d_2)\bar{\mathbf{M}}_{21}\mathbf{e}_1(-d_2^+) = \bar{\mathbf{M}}_{11}\mathbf{e}_1(-d_2^+),$$

$$\mathbf{e}_1(-d_2^+) = \mathbf{v} + \mathbf{e}_1(-d_2^-),$$

$$\mathbf{e}_1(-d_2^-) = \bar{\mathbf{M}}_{13}\bar{\mathbf{M}}_3(d_3)\bar{\mathbf{M}}_{34}\mathbf{e}_4(-d),$$

where

$$\bar{\mathbf{M}}_{11} = \bar{\mathbf{M}}_{12}\bar{\mathbf{M}}_2(d_2)\bar{\mathbf{M}}_{21}. \tag{17}$$

The emitted SHG field above the system may then be found through algebraic substitution as described before. The results are the same as Eq. (16) but with the t replaced by b, and coefficients given in Table II. The variable $\tilde{e}_{1\pm}(-d_2)$ refers to the upward (+) or downward (−) propagating E-field at the top vacuum interface. The tilde (used here and below) indicates that it is normalized to the incident E-field so that the coefficients given are entirely unitless.

The final contribution is from the Si, which is treated phenomenologically here. From symmetry considerations, it is known that the total E-field produced from Si(001) (dipolar and quadrupolar contributions) is fourfold symmetric, and the s-polarized SHG E-field has no isotropic contribution.[10] For linearly g-polarized (g is s or p) fundamental light it is assumed that the h-polarized (h is s or p) SHG E-field $E_{gh}^{2\omega}$ from the silicon depends on the downward propagating g-polarized E-field in the SiO$_2$/Si interface $e_{1-}^g(-d)$,

TABLE II. Radiated E-field coefficients from C-film/SiO$_2$ interface.

$$c_{b,11}^{ss} = \left(M_{11s}^{1,1} - \frac{M_{14s}^{1,2}M_{11s}^{2,1}}{M_{14s}^{2,2}} - M_{11s}^{1,2} + \frac{M_{14s}^{1,2}M_{11s}^{2,2}}{M_{14s}^{2,2}}\right)[\tilde{e}_{1+}^{s}(-d_2) + \tilde{e}_{1-}^{s}(-d_2)]^2$$

$$c_{b,11}^{ps} = -\left(M_{11s}^{1,1} - \frac{M_{14s}^{1,2}M_{11s}^{2,1}}{M_{14s}^{2,2}} - M_{11s}^{1,2} + \frac{M_{14s}^{1,2}M_{11s}^{2,2}}{M_{14s}^{2,2}}\right)[\tilde{e}_{1-}^{p}(-d_2) - \tilde{e}_{1+}^{p}(-d_2)]^2\cos^2(\theta)$$

$$b_{b,11}^{sp} = -\left(-M_{11p}^{1,1} + \frac{M_{14p}^{1,2}M_{11p}^{2,1}}{M_{14p}^{2,2}} - M_{11p}^{1,2} + \frac{M_{14p}^{1,2}M_{11p}^{2,2}}{M_{14p}^{2,2}}\right)\cos(\theta)[\tilde{e}_{1+}^{s}(-d_2) + \tilde{e}_{1-}^{s}(-d_2)]^2$$

$$b_{b,11}^{pp} = \left(-M_{11p}^{1,1} + \frac{M_{14p}^{1,2}M_{11p}^{2,1}}{M_{14p}^{2,2}} - M_{11p}^{1,2} + \frac{M_{14p}^{1,2}M_{11p}^{2,2}}{M_{14p}^{2,2}}\right)[\tilde{e}_{1-}^{p}(-d_2) - \tilde{e}_{1+}^{p}(-d_2)]^2\cos^3(\theta)$$

$$a_{b,31}^{sp} = \left(M_{11p}^{1,1} - \frac{M_{14p}^{1,2}M_{11p}^{2,1}}{M_{14p}^{2,2}} - M_{11p}^{1,2} + \frac{M_{14p}^{1,2}M_{11p}^{2,2}}{M_{14p}^{2,2}}\right)\sin(\theta)[\tilde{e}_{1+}^{s}(-d_2) + \tilde{e}_{1-}^{s}(-d_2)]^2$$

$$a_{b,31}^{pp} = \left(M_{11p}^{1,1} - \frac{M_{14p}^{1,2}M_{11p}^{2,1}}{M_{14p}^{2,2}} - M_{11p}^{1,2} + \frac{M_{14p}^{1,2}M_{11p}^{2,2}}{M_{14p}^{2,2}}\right)[\tilde{e}_{1-}^{p}(-d_2) - \tilde{e}_{1+}^{p}(-d_2)]^2\cos^2(\theta)\sin(\theta)$$

$$a_{b,33}^{pp} = \left(M_{11p}^{1,1} - \frac{M_{14p}^{1,2}M_{11p}^{2,1}}{M_{14p}^{2,2}} - M_{11p}^{1,2} + \frac{M_{14p}^{1,2}M_{11p}^{2,2}}{M_{14p}^{2,2}}\right)[\tilde{e}_{1+}^{p}(-d_2) + \tilde{e}_{1-}^{p}(-d_2)]^2\sin^3(\theta)$$

$$a_{b,15}^{pp} = 2\left(-M_{11p}^{1,1} + \frac{M_{14p}^{1,2}M_{11p}^{2,1}}{M_{14p}^{2,2}} - M_{11p}^{1,2} + \frac{M_{14p}^{1,2}M_{11p}^{2,2}}{M_{14p}^{2,2}}\right)$$
$$\times[\tilde{e}_{1-}^{p}(-d_2) - \tilde{e}_{1+}^{p}(-d_2)]\cos^2(\theta)[\tilde{e}_{1+}^{p}(-d_2) + \tilde{e}_{1-}^{p}(-d_2)]\sin(\theta)$$

TABLE III. Fourier elements of the total SHG intensity.

$$f_{pp}^{0} = |\beta_{pp}s_{pp} + a_{31}^{pp}\partial_{31} + a_{33}^{pp}\partial_{33} + a_{15}^{pp}\partial_{15}|^2 + \frac{|\alpha_{pp}s_{pp}|^2}{2} + \frac{|b_{11}^{pp}\partial_{11}|^2}{2}$$

$$f_{pp}^{3} = 2\Re[(\beta_{pp}s_{pp} + a_{31}^{pp}\partial_{31} + a_{33}^{pp}\partial_{33} + a_{15}^{pp}\partial_{15})(b_{11}^{pp}\partial_{11})^*]$$

$$f_{pp}^{6} = \frac{|b_{11}^{pp}\partial_{11}|^2}{2}$$

$$f_{sp}^{0} = |\beta_{sp}s_{sp} + a_{31}^{sp}\partial_{31}|^2 + \frac{|\alpha_{sp}s_{sp}|^2}{2} + \frac{|b_{11}^{sp}\partial_{11}|^2}{2}$$

$$f_{sp}^{3} = 2\Re[(\beta_{sp}s_{sp} + a_{31}^{sp}\partial_{31})(b_{11}^{sp}\partial_{11})^*]$$

$$f_{sp}^{6} = \frac{|b_{11}^{sp}\partial_{11}|^2}{2}$$

$$f_{ps}^{0} = \frac{|s_{ps}\alpha_{ps}|^2}{2} + \frac{|c_{11}^{ps}\partial_{11}|^2}{2}$$

$$f_{ps}^{6} = -\frac{|c_{11}^{ps}\partial_{11}|^2}{2}$$

$$f_{ss}^{0} = \frac{|s_{ss}\alpha_{ss}|^2}{2} + \frac{|c_{11}^{ss}\partial_{11}|^2}{2}$$

$$f_{ss}^{6} = -\frac{|c_{11}^{ss}\partial_{11}|^2}{2}$$

$$E_{gs}^{2\omega} = \frac{iK^2}{2K_z\varepsilon_0}\alpha_{gs}\sin(4\phi)[e_{1-}^{g}(-d)]^2,$$

$$E_{gp}^{2\omega} = \frac{iK^2}{2K_z\varepsilon_0}[\beta_{gp} + \alpha_{gp}\cos(4\phi)][e_{1-}^{g}(-d)]^2. \quad (18)$$

The α and β are phenomenological constants accounting for both the surface and bulk contributions and are complex valued. The angle ϕ is taken relative to the [100] direction in the Si. The SHG light is treated as originating from the top of the Si, and must propagate through the system. From Eq. (5), and solving for the transmitted E-field to the top surface, T_{41}, the radiated SHG from the Si may be written as

$$\frac{E_{gs}^{2\omega}}{(E_g^\omega)^2} = \frac{iK^2}{2K_z\varepsilon_0}s_{gs}\alpha_{gs}\sin(4\phi),$$

$$\frac{E_{gp}^{2\omega}}{(E_g^\omega)^2} = \frac{iK^2}{2K_z\varepsilon_0}[\beta_{gp} + \alpha_{gp}\cos(4\phi)]s_{gp},$$

where

$$s_{gh} = \left(M_{14,h}^{1,1} - \frac{M_{14,h}^{2,1}M_{14,h}^{1,2}}{M_{14,h}^{2,2}}\right)[\tilde{e}_{1-}^{g}(-d)]^2. \quad (19)$$

The unitless parameter s_{gh} incorporates all the linear optical properties for the fundamental and SHG fields in the multilayer structure.

D. Total SHG intensity

All of the SHG E-fields have now been evaluated at the top surface of the system, and written in terms of the linear optical properties, propagation distances, and nonlinear susceptibilities. These fields must be added coherently to find the SHG intensity. The C-film SHG coefficients from the top and bottom surfaces add together ($c_{t,11}^{ss} + c_{b,11}^{ss} = c_{11}^{ss}$, etc.),

along with the SHG from the substrate. The C-film is generally placed on the substrate at a random angle δ relative to the [100] direction of the substrate. The resultant SHG intensity $I_{gh}^{2\omega}(\phi)$ may be analyzed in terms of Fourier components,

$$\frac{I_{gh}^{2\omega}(\phi)}{(I_g^\omega)^2} = |F^2|\sum_m f_{gh}^{m}\cos m(\phi - \delta_m), \quad (20)$$

where the incident and outgoing polarizations are g and h, respectively, and the Fourier elements f_{gh}^{m} are constants dependent on the number of layers. When the isotropic, threefold, and fourfold contributions add (modulus squared), they generate other Fourier elements (0,1,3,4,6,7,8) with a phase shift dependent on the sample orientation (i.e., $\delta_3 = \delta_6 = \delta$ and $\delta_0 = \delta_4 = 0$). Because the fourfold contribution from the Si is significantly weaker than its isotropic contribution and the C-film's threefold contribution (as shown in Secs. III and IV), the strongest remaining elements are 0,3, and 6.[10,15] These Fourier elements are shown in Table III.

This gives the SHG intensity Fourier components in terms of the C-film nonlinear tensor elements (∂_x), calculable linear parameters (a, b, c, and s) which depend on the number of layers, and the effective nonlinear parameters of Si (α, β). The linear parameters may be numerically calculated as described above. Although this involves complex matrix calculations, the final results are unitless numbers that depend on the number of layers. Some of these are shown in Figs. 2 and 3 for the parameters used in the experiment described here (fundamental wavelength of 800 nm, 60° angle of incidence, and sample structure described above).

Several patterns may be noted from the constants a, b, and c which effectively give weight to the nonlinear tensor elements (∂_x). Those for ∂_{11} are all greatest for two layers, and decay with thickness (as shown in Fig. 2). This is the element which gives the threefold symmetry as shown in Eq. (10). All others (for ∂_{31}, ∂_{33}, ∂_{15}) are weakest for two layers, and increase with C-film thickness (as shown in Fig. 3). These elements give an isotropic contribution which adds to that from the substrate, which will have a contribution which decreases with C-film thickness. These observations agree with those inferred in the thin-film limit: the strongest threefold SHG will result from bilayer graphene, and the aniso-
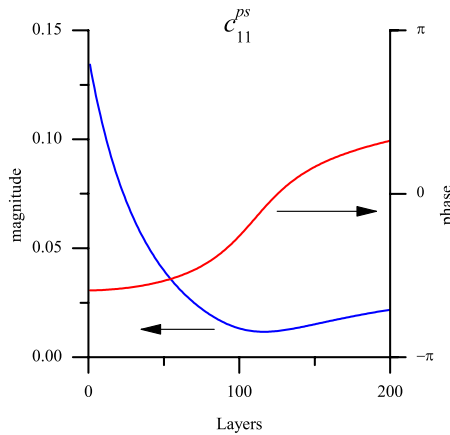
FIG. 2. (Color online) Magnitude (blue) and phase (red) of c_{11}^{ps} vs number of layers. The contributions to the SHG from the top and bottom surfaces of the C-film add constructively for thin samples.

tropy will decrease with thicker C-films. The variation in the magnitude of the isotropic response with C-film thickness is not obvious because the contribution from the C-film will increase, and the contribution from the substrate will decrease for thicker films.

Once the linear parameters are incorporated, the Fourier elements f_{gh}^m only depend on the C-film and substrate nonlinear tensor elements ∂_x, α, and β. This suggests the use of simple fitting to find the tensor elements.

The fourfold anisotropy of the substrate is very weak compared to that from the C-film, thus for qualitative discussion, α may be ignored, and the phase of the substrate SHG with the p-in, p-out combination may be taken to be real.[15] Of particular note is that the (ps) and (ss) polarization combinations involve only the ∂_{11} tensor element. Therefore, this can be determined to within a phase factor. For sufficiently thin samples, both (pp) and (sp) combinations involve only the ∂_{11} and β_{pp} or β_{sp} elements; therefore the phase of ∂_{11} may be determined. With thicker samples, using the (sp) combination, only ∂_{11} and ∂_{31} contribute; therefore the magnitude and phase of ∂_{31} may be found from the zeroth and third Fourier elements (and for thin samples, the magnitude
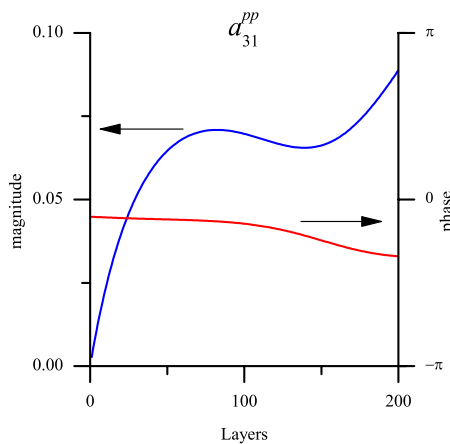

FIG. 3. (Color online) Magnitude (blue) and phase (red) of a_{31}^{pp} vs number of layers. The contributions to the SHG from the top and bottom surfaces of the C-film add destructively for thin samples.

and phase of β_{ps} may then be found if desired). Finally, the (pp) polarization combination involves both of these and ∂_{33} and ∂_{15}, which leaves some ambiguity in solving for both of the latter.

The theory described above applies only for s/p incident, and s/p observed polarization but a similar analysis can also be used for diagonally polarized incident light with observed s polarization (ds). This case is more complex because, as suggested by Eq. (10), the generated E-field has a complex term proportional to $\sin(3\phi)$, and a complex term proportional to $\cos(3\phi)$. The corresponding threefold symmetry will therefore have a magnitude and phase shift involving both terms. These may be calculated in the same way as the other polarization combinations but is not explicitly shown here. Since the P_y polarization is observed, and it is generated by E-fields along x, y, and z, Eq. (10) shows that only the ∂_{11} and ∂_{15} tensor elements are involved (for thicker samples, where the substrate is blocked). Thus, from the zeroth and third Fourier elements (and confirmed through the phase of the third element) the magnitude and phase of ∂_{15} may be found. Finally, ∂_{33} may be found through the (pp) combination.

III. EXPERIMENT

The SHG experiments were performed with exfoliated C-films on a 300 nm oxidized Si(001) substrate. This allowed the samples to be imaged optically and the number of layers determined as discussed previously. The fundamental beam is derived from a Ti:sapphire oscillator providing 1.0 nJ, 150 fs pulses with a center wavelength of 800 nm. These pulses are attenuated to ~0.06 nJ to avoid damaging the samples, and focused onto the samples using a 0.12 numerical aperture microscope objective, generating an elliptical spot size of approximately 7 μm $\times$ 10 μm. An angle of incidence of θ=60° is used for all experiments. The 400 nm SHG light is collected using an off-axis parabolic mirror and separated from the fundamental light using a prism, and further optically filtered before being measured with a cooled photomultiplier tube and photon-counting electronics. The samples are positioned on a set of translation and rotation stages such that they can be rotated about the surface normal while keeping a particular point in the beam focus. A half-wave plate and polarizer are used to control the polarization state of the fundamental light, and an additional polarizer was used to select which SHG polarization to measure. All four combinations of s- and p-polarized fundamental and SHG light are measured, as well as diagonal-in, and s-out for reasons described above.

The samples are imaged optically in a confocal arrangement on a charge coupled device camera to maintain the position of the focal spot relative to the samples. The position of the axis of the rotation stage is only well defined to within ~10 μm. Thus, samples of diameter >20 μm are used to avoid situations where the focal spot would drift off the sample during rotation. It is often found, however, that slightly different positions on a sample would give different SHG intensities, due to imperfect crystal structure, glue from the exfoliation process, or other sample inhomogeneities.
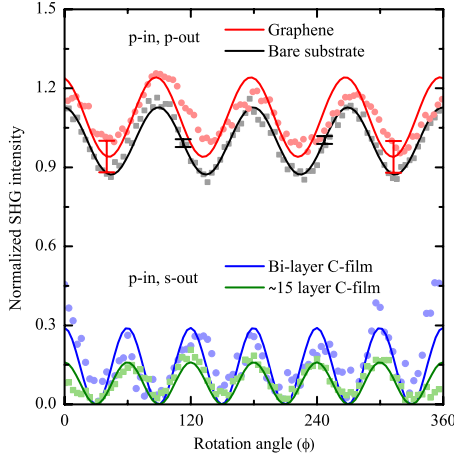
FIG. 4. (Color online) Normalized SHG signal as a function of rotation angle ϕ. Top two curves: (pp) data for the bare substrate (black squares, lower curve) and graphene (red circles, upper curve), both fit to $A + B \cos 4\phi$ as suggested by Eq. (19). Lower two curves: (ps) data for a bilayer sample (blue circles, upper curve), and a ∼15-layer sample (green squares, lower curve), both fit to $A \cos^2(3\phi)$ [as suggested by Eq. (16)]. The absolute angle is the same for the (pp) curves but is otherwise arbitrary.

These variations appear in Figs. 4 and 5 as deviations in the data from the fit. Since the SHG intensity is very weak (a few photons per second), data was averaged over many rotations of the sample to improve signal/noise.

IV. RESULTS AND ANALYSIS

Figure 4 shows the (pp) polarized SHG intensity from the bare substrate and from graphene, both normalized to the square of the incident intensity, and such that the average signal from the substrate is taken to be unity. Over the course
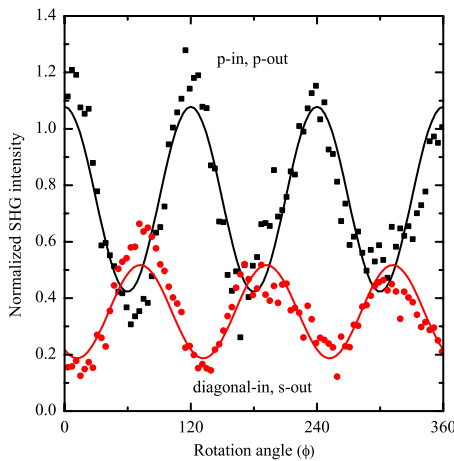

FIG. 5. (Color online) For a ∼5-layer sample, both (pp) (black squares) and (ds) (red circles) polarization combinations are shown. The absolute angle is arbitrary, but is the same in both plots. Both data sets are fit to $A + B \cos(3\phi + \phi_0)$ and are normalized such that the isotropic component of the SHG signal from the substrate would be unity. The phase shift ($\phi_0 \approx 144°$) associated with (ds) relative to (pp) is evident.

of several measurements, it was found that the SHG from graphene is at best marginally stronger than that from the bare substrate. However, we do not attempt to extract tensor information from these results because the experimental uncertainty does not warrant it.

Results for (ps) SHG are also shown in Fig. 4 for a bilayer and ∼15-layer sample. It is clear that the sixth Fourier element decreases with layer number. Results for (ss) polarization combinations are qualitatively similar. Two data sets from a ∼5-layer sample are shown in Fig. 5—one with (pp) and one with (ds). The third Fourier element always has the same phase between (pp) and (sp) combinations, and inverted negative for (ps) and (ss) combinations as is shown in Table III but is evidently shifted with diagonal polarization.

Although for each sample and polarization combination, the SHG intensity was measured for many angles ϕ, the only useful parameter values that may be extracted are the first few elements in the Fourier series of $I_{2\omega}(\phi)$. Because the fourfold contribution from the substrate is much weaker than the threefold contribution from the C-film, only the zeroth, third, and sixth elements are consistently larger than the noise. In cases where there is a large third element [(pp), (sp), (ds) polarization combinations], the sixth element is too weak to be seen. This pattern is comparable to that from bare Si(001); when the isotropic contribution is polarization suppressed, an apparent eightfold symmetry arises due to the fourfold symmetric E-field squared but when the isotropic contribution is allowed, the interference between the (strong) isotropic and (weak) fourfold E-field contributions gives a fourfold symmetric signal with an unmeasurable weak eightfold component. Finally, neglecting the weak Si contribution, the signal from the (ss) and (ps) combinations is of the form $\sin^2(3\phi)$ so the zeroth element and sixth element provide the same information. Therefore, the most important Fourier elements of the data are shown in Fig. 6. The intensity is normalized such that the zeroth (isotropic) Fourier element from the Si/SiO_2 substrate is unity. When multiple samples of the same thickness were available, the average was used, and the error bars represent the variation. A few data points vary significantly from the fit, and likely result from sample imperfections where too few samples of the same thickness were available to average over.

The trends in the data confirm those suggested in Figs. 4 and 5. The strongest anisotropic SHG occurs for bilayer graphene and generally decreases with increasing C-film thickness. The isotropic contribution behaves in a similar manner for most polarization combinations. This is in agreement with the theoretical predictions which assume interference between SHG polarization sheets on either side of the C-film, and hence that an inversion symmetry argument does not apply for thin films. The extremely weak SHG from graphene is also in agreement with the theory which predicts destructive interference between the two interfacial SHG sources.

The data is fit to the parameters shown in Table III for the four complex parameters ∂_x. This effectively involves choosing values for all four ∂_x to minimize the difference between the theoretical and experimental Fourier components f_{gh}^m. These nonlinear tensor elements are
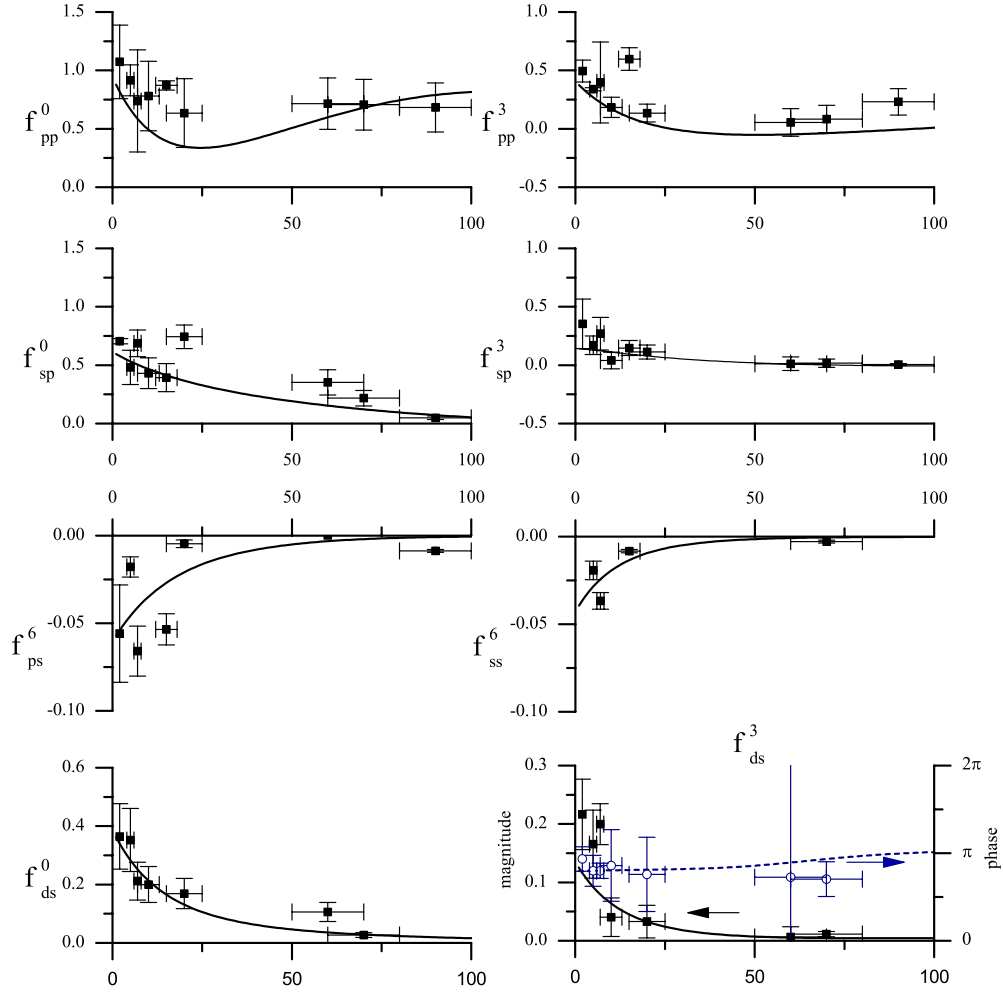
FIG. 6. (Color online) Fourier elements of $I_{2\omega}(\phi)$ for various polarization combinations: (top-left and right: zeroth and third element for (pp); second from top left and right: zeroth and third element for (sp); third from top left: sixth element for (ps); right: sixth element for (ss); bottom left and right: zeroth and third element for (ds) where the phase of the third Fourier element has been plotted as well). The x axis is the number of layers of graphene in each graph. The SHG intensity has been normalized to the square of the incident intensity, and normalized such the isotropic contribution from the bare SiO_2/Si substrate is unity. The curves are fits using the equations in Table III.

$$\partial_{11} = 0.6 + 2.4i,$$

$$\partial_{15} = 0.2 - 0.7i,$$

$$\partial_{31} = -0.5 + 5.2i,$$

$$\partial_{33} = -0.17 + 0.19i. \qquad (21)$$

These values are normalized such that the (pp) SHG signal generated from the Si/SiO_2 substrate is unity, the phase of β_{pp} is chosen to be zero, and the constant $|F^2| = 1$ in Eq. (20). For all values the radius of the uncertainty circle in the complex plane is estimated to be about 25% of the modulus of the coefficient.

It is worth emphasizing that the use of the four nonlinear tensor elements associated with the dipolar contribution from a single graphene/air interface is sufficient to account for the trends in the data. It is particularly interesting that, as in the case of linear optical propagation, no material constants have to be changed in going from two layers to bulk; only the

C-film thickness needs to be changed in the calculations. If a bulk quadrupolar contribution from the C-films exists, it must be weak and, in any event, does not seem to be needed to account for the variation in the SHG signal with number of layers. Variations in the SHG signal with number of layers is mainly accounted for by linear light propagation effects, once multilayer interference is taken into account.

V. CONCLUSIONS

In summary, we have provided a theoretical foundation and experimental data for the polarization and azimuthal angular dependence of the SHG from graphene and few-layer graphitic films on a SiO_2/Si substrate for various polarization combinations. All these data can be understood on the basis of the linear optical properties of the thin-film system, the SHG response of the silicon, and the four nonzero nonlinear dipolar tensor elements of a single air/graphene interface. Values for these latter parameters were obtained relative to that of the silicon substrate. We explain why the

graphene itself shows zero anisotropic response and negligible isotropic response through near complete cancellation of SHG sources on both sides of the film. We also show why bilayer graphene and all other films possess a sufficiently strong anisotropic response, effectively suppressing the fourfold symmetry of the SHG from the underlying Si substrate. All variation in the SHG signal from bilayer graphene to bulk graphite can be accounted for on the basis of linear propagation, including interference, effects. Bulk quadrupolar effects in the C-films, which at most can give rise to an isotropic contribution to SHG, appear to be negligible.

*jdean@physics.utoronto.ca

[1] P. Blake, E. W. Hill, A. H. C. Neto, K. S. Novoselov, D. Jiang, R. Yang, T. J. Booth, and A. K. Geim, Appl. Phys. Lett. **91**, 063124 (2007).

[2] D. S. L. Abergel, A. Russell, and V. I. Fal'ko, Appl. Phys. Lett. **91**, 063125 (2007).

[3] K. S. Novoselov, A. K. Geim, S. V. Morozov, D. Jiang, Y. Zhang, S. V. Dubonos, I. V. Grigorieva, and A. A. Firsov, Science **306**, 666 (2004).

[4] C. Berger, Z. Song, T. Li, X. Li, A. Y. Ogbazghi, R. Feng, Z. Dai, A. N. Marchenkov, E. H. Conrad, P. N. First, and W. A. de Heer, J. Phys. Chem. B **108**, 19912 (2004).

[5] J. Hass, R. Feng, J. E. Millán-Otoya, X. Li, M. Sprinkle, P. N. First, W. A. de Heer, E. H. Conrad, and C. Berger, Phys. Rev. B **75**, 214109 (2007).

[6] A. C. Ferrari, J. C. Meyer, V. Scardaci, C. Casiraghi, M. Lazzeri, F. Mauri, S. Piscanec, D. Jiang, K. S. Novoselov, S. Roth, and A. K. Geim, Phys. Rev. Lett. **97**, 187401 (2006).

[7] M. A. Pimenta, G. Dresselhaus, M. S. Dresselhaus, L. G. Cançado, A. Jorio, and R. Saito, Phys. Chem. Chem. Phys. **9**, 1276 (2007).

[8] J. M. Dawlaty, S. Shivaraman, M. Chandrashekhar, F. Rana, and M. G. Spencer, Appl. Phys. Lett. **92**, 042116 (2008).

[9] R. W. Newson, J. Dean, B. Schmidt, and H. M. van Driel, Opt. Express **17**, 2326 (2009).

[10] H. W. K. Tom, T. F. Heinz, and Y. R. Shen, Phys. Rev. Lett. **51**, 1983 (1983).

[11] J. E. Sipe, D. J. Moss, and H. M. van Driel, Phys. Rev. B **35**, 1129 (1987).

[12] Y. R. Shen, Nature (London) **337**, 519 (1989).

[13] J. I. Dadap, B. Doris, Q. Deng, M. C. Downer, J. K. Lowell, and A. C. Diebold, Appl. Phys. Lett. **64**, 2139 (1994).

[14] S. T. Cundiff, W. H. Knox, F. H. Baumann, K. W. Evans-Lutterodt, M.-T. Tang, M. L. Green, and H. M. van Driel, Appl. Phys. Lett. **70**, 1414 (1997).

[15] J. J. Dean and H. M. van Driel, Appl. Phys. Lett. **95**, 261910 (2009).

[16] J. E. Sipe, J. Opt. Soc. Am. B **4**, 481 (1987).

[17] J. J. H. Gielis, P. M. Gevers, I. M. P. Aarts, M. C. M. van de Sanden, and W. M. M. Kessels, J. Vac. Sci. Technol. A **26**, 1519 (2008).

[18] *Handbook of Optical Constants of Solids*, edited by E. D. Palik (Academic Press, New York, 1991), Vol. 2, pp. 449–460.